EP-DT
Detector Technologies

CERN Summer Student Programme

Research on environmentally friendly gases for particle detectors

---

Design and fabrication of a glass multigap RPC prototype to evaluate eco-friendly gas mixtures

---

Author
Sahna BELBAGRA[1]
[1] *Mines de Nancy*

Supervisors
Mattia VERZEROLI
Beatrice MANDELLI

Project Report

September 2025

Abstract

This report focuses on the design of a new MRPC prototype that routes the working gas around the detector rather than only inside it, in order to mitigate overpressure issues. The project comprised the mechanical design, fabrication and testing of two identical prototypes, followed by data analyses including current (I–V) scans, detection efficiency, time-resolution studies and general characterization. The resulting prototype is intended as a platform to evaluate environmentally friendly (low-GWP) gas mixtures and to assess whether comparable performance can be achieved with greener gases.

Contents

I Introduction **3**
I.1 MRPC detectors at CERN . . . 3
I.2 Greenhouse gases at CERN . . . 3
I.3 Gas mixture alternatives . . . 4

II Modeling and Prototype Construction **5**
II.1 3D Modelling and Drawings . . . 5
II.2 Building every layers . . . 6
II.2.1 Glass with graphite varnish . . . 6
II.2.2 Glass layer and copper strips . . . 7
II.3 Assembly of the MRPC Module . . . 7
II.3.1 Surface Preparation . . . 7
II.3.2 Gluing and Stack Build-Up . . . 8
II.3.3 Gas Interfaces and Readout Interconnects . . . 8
II.3.4 Final Closure and Sealing . . . 9

III Detector Analysis **10**
III.1 Experimental setup . . . 10
III.1.1 Scintillator calibration . . . 10
III.1.2 Detector installation in the setup . . . 11
III.2 Weekly current scan and detector conditioning . . . 11
III.3 Efficiency analysis . . . 12
III.3.1 Method . . . 12
III.3.2 Results . . . 12
III.3.3 Operational limit and interpretation . . . 13
III.4 Disassembly, Inspection, and Corrective Actions . . . 13
III.4.1 Findings on MRPC1: bottom-glass fracture . . . 13
III.4.2 Findings on MRPC2: non-uniform gaps and discharge hypothesis . . . 13
III.4.3 Corrective actions and reassembly . . . 14
III.4.4 Post-repair tests . . . 14
III.4.5 Next steps . . . 15
III.5 Comparison of detectors . . . 15
III.5.1 Design differences . . . 15
III.5.2 Installation and commissioning . . . 15
III.5.3 Current scan . . . 16
III.5.4 Efficiency scan . . . 16
III.5.5 Interpretation and next steps . . . 16

IV Future Work and Proposed Solutions **17**
IV.1 Prototype assessment and design implications . . . 17
IV.1.1 Strengths and limitations of the prototype . . . 17
IV.1.2 Design priorities for the next prototype . . . 17
IV.2 Design improvements for future prototypes . . . 18
IV.2.1 Motivation . . . 18
IV.2.2 Proposed assembly concept . . . 18
IV.2.3 Concept of a 3D-printed support frame . . . 19

V Conclusion **20**

I Introduction

I.1 MRPC detectors at CERN

First outlined in 1996 by M. C. S. Williams and collaborators [1], the Multigap Resistive Plate Chamber (MRPC) extends the classical RPC concept by carving the gas volume into a stack of several thin sub-gaps. The stack is formed by alternating resistive plates; only the two outer electrodes are connected to high voltage, while the internal plates are left electrically floating so that a uniform electric field is established independently in each sub-gap (see Fig. 1a). This architecture preserves the simplicity and robustness of RPCs while enabling operation at lower gain and with improved timing.

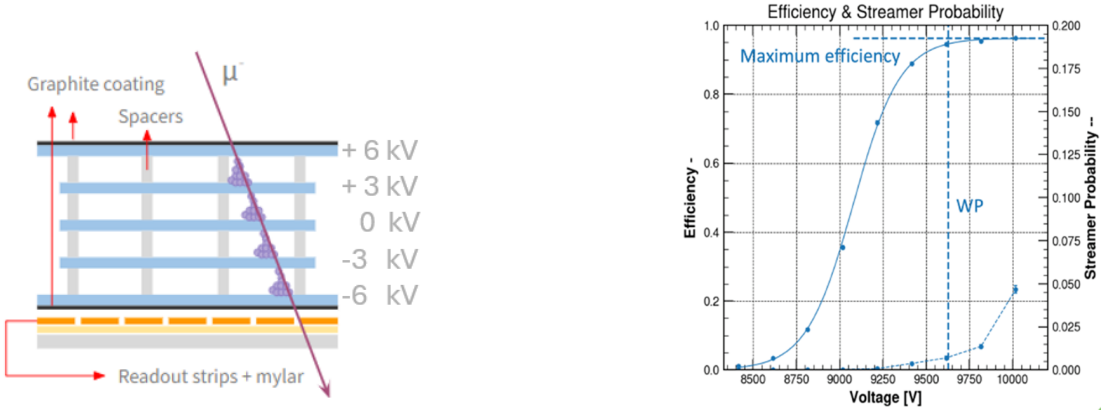

(a) Transversal section of an MRPC.

(b) Efficiency plot.

Figure 1: Overview of the detector and an expecting efficiency plot.

When an ionizing particle passes through the chamber, it creates ion–electron pairs in each small gap. With high voltage applied, the electrons drift to the anode and can start avalanches if the field is strong enough. The moving charges make a signal on the readout strips placed near the outer glass plates. The readout is separated from the resistive coating by an insulator, so we can pick up the signal without drawing current from the high-voltage electrodes.

The multigap design makes many small avalanches occur at the same time in different gaps. Even if one avalanche is too small to detect, their signals add up at the readout and cross the threshold. This gives a stronger, cleaner pulse at lower voltage, improves detection efficiency (see Fig. 1b) and allows good timing, one reason why MRPCs are useful in modern trigger and timing systems.

I.2 Greenhouse gases at CERN

Greenhouse gases warm the planet by absorbing and re-emitting infrared radiation. Even though they are only a small part of the air, they strongly influence Earth's energy balance. The main gases in this group are carbon dioxide (CO_2), methane (CH_4), water vapor and nitrous oxide (N_2O). Their amounts change with natural processes (like vegetation and geology) and with human activity, most notably the burning of fossil fuels since the Industrial Revolution.

To compare their climate impact, we use Global Warming Potential (GWP), which tells us how much heat a gas traps over a set time compared to CO_2. Some industrial gases stand out: HFCs and SF_6 have extremely high GWPs because they absorb infrared very effectively and stay in

the atmosphere for a long time. These gases mostly come from industry and were not present in the pre-industrial atmosphere.

Because of their impact,the European Union's F-gas rules aim to cut fluorinated-gas emissions to 70% percent below 1990 levels by 2030. The legislation reduces HFCs and restricts SF_6 which has a GWP of about 23 900 and under Regulation (EU) 2024/573, pushes a gradual phase-out in favor of safer alternatives, with strict requirements for handling and disposal [2].

Since the Kyoto Protocol,EU policies have led to large cuts in F-gas use [3]. From 2015, an HFC quota system reduced market supply and encouraged low-GWP HFOs. The EU's long-term plan is to end HFC sales by 2050 as part of its climate-neutrality goal. Other measures tighten leak prevention, add digital monitoring and enforcement and require certified training for anyone working with F-gases.

CERN contributes to these efforts [4]. The actions taken to reduce detector gas emissions mean that the tCO_2e at the start of LHC Run3 is lower than in Run2. To manage consumption and emissions in a practical way, the EP-DT-FS Gas group has defined several levels of intervention and corresponding actions [5].

Four strategies have been defined to improve gas use at CERN:

- Gas recirculation systems
- Gas recuperation systems
- Research on environmentally friendly gases for particle detectors

During my project, I worked on the third strategy, as my goal was to build a prototype MRPC detector to test new gas mixtures.

I.3 Gas mixture alternatives

HPL RPC detectors typically use a three-component gas blend of about 95.2% R134a, 4.5% isobutane (iC_4H_{10}) and 0.3% SF_6. This mix is operationally stable, but both R134a (an HFC) and SF_6 have high global warming potential (GWP). For glass MRPCs, the reference mixture is similar: 93% R134a, 5% isobutane and 2% SF_6, to keep high efficiency and excellent time resolution.

Gas	Alternative to	GWP
R134a	–	1430
SF_6	–	23900
iC_4H_{10}	–	3.3
CO_2	R134a	1
HFO-1234ze	R134a	<1
NOVEC 4710	SF_6	2100

Figure 2: Global Warming Potential (GWP) for baseline gases and proposed alternatives.

To reduce the carbon footprint, several alternatives are being studied to replace all or part of R134a. For example, in HPL RPC, several test where made to substitute R134a with: ∼30%

CO_2 blends (already used in long-term operation in ATLAS), very-low-GWP HFOs such as HFO-1234ze (GWP < 1) or R1336mzz (GWP ≈ 2) and other compatible diluents (He, Ar, R32, N_2, CO_2). In parallel, SF_6 substitutes are also under evaluation, notably NOVEC 4710, which has a GWP of 2100 (see Fig. 2). Because the main issue for MRPCs is their high SF_6 concentration and since NOVEC 4710 performs well in HPL RPCs, we also tested it in MRPCs. These options require adjusting of operating conditions (HV, thresholds, timing) and validation campaigns in the lab and over long runs, while ensuring compatibility with LHC gas systems and maintaining key MRPC performance (efficiency plateau, noise, stability and time resolution).

II Modeling and Prototype Construction

II.1 3D Modelling and Drawings

The project aimed to build two identical MRPC detectors so they could be tested separately and in parallel. I started with hand sketches to explore layouts and assembly options. Once a viable concept emerged, I created a parametric 3D model in *Autodesk Inventor Professional*. The assembly includes all critical parts—glass electrodes, spacers, frames, inlet/outlet fittings, readout strips so that clearances, tolerances and cable paths can be checked in context. Top-down constraints ensure both detectors are geometrically identical and simplify later design iterations.

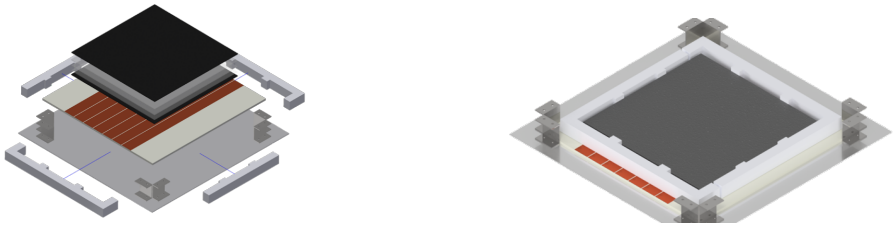

(a) Exploded view of the MRPC prototype.

(b) Assembled view.

Figure 3: MRPC prototype model

The CAD model served as a reference for manufacturing. From it, detailed 2D drawings were produced for each part and for the full assembly: dimensions, hole spot, size of the spacers and an assembly drawing with an exploded view (Fig. 3). For the machined and cut plates, DXF profiles have been exported directly from Inventor for water-jet cutting of the supports (Fig. 4a).

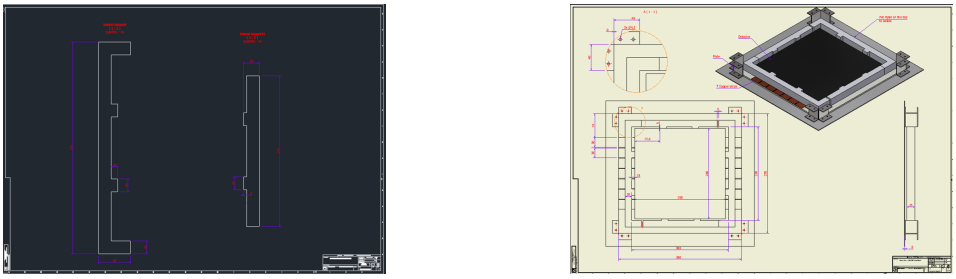

(a) DXF profiles for water-jet cutting.

(b) Assembly drawing with key dimensions.

Figure 4: Manufacturing documentation

This 3D and drawing workflow was essential to lock down the detector design before procurement, define an unambiguous build sequence (jigs, alignment pins and glue steps) and provide a clean baseline for future changes. Any future modification: geometry, materials or gas interfaces can be implemented once in the model and automatically propagated to the drawings, ensuring that both detectors remain strictly identical.

II.2 Building every layers

II.2.1 Glass with graphite varnish

The goal is to apply a graphite layer on the two future detectors external glasses to apply the high voltage needed for their operation. We start with preparation: clean the surfaces with alcohol and water, then dry them quickly to avoid marks. Next, a conductive graphite varnish is applied to one side of each plate using an airbrush (a small spray gun often used in model making) to deposit a thin, even coat. The key is to obtain a homogeneous, continuous layer: thickness uniformity controls the field uniformity and high-voltage stability (Fig. 5a). The plates are then left to dry for 24 hours.

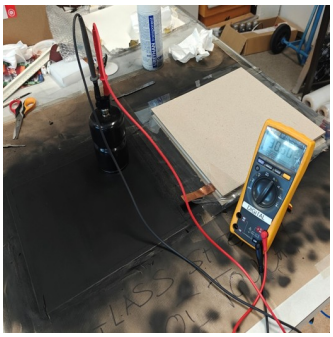

(a) Surface–resistivity measurement with probe and multimeter.

400 kΩ/cm^2	510 kΩ/cm^2	560 kΩ/cm^2
410 kΩ/cm^2	560 kΩ/cm^2	500 kΩ/cm^2
320 kΩ/cm^2	430 kΩ/cm^2	430 kΩ/cm^2

(b) Resistivity map over a grid of points.

Figure 5: Test of the graphite-coated glass

After drying,surface resistivity is checked by mapping a grid of points. Typical values are around 320–560 kΩ /cm^2, which indicates a well-formed layer (Fig. 5b). This step helps identify areas that are too resistive (poor coverage) or too conductive (local overloads) and validates the electrode before assembly.

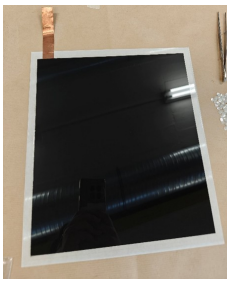

Figure 6: Glass plate with graphite coating, insulating varnish and copper contact tab.

The graphite surface is then protected with a clear insulating varnish (urethane). This layer protects the conductive paint mechanically and electrically insulates it from the environment, limiting leakage currents and wear during handling (Fig. 6).

Finally, the electrical connection is added: a copper strip is bonded to the contact area using a conductive epoxy.

II.2.2 Glass layer and copper strips

The goal of this step is to build the layers located between the two graphite-coated electrodes: a glass plate fitted with spacers that set the MRPC gap thicknesses. I also prepare the readout plane, made of copper strips bonded onto a Mylar film. The whole assembly must be geometrically clean, repeatable and compatible with the final stack.

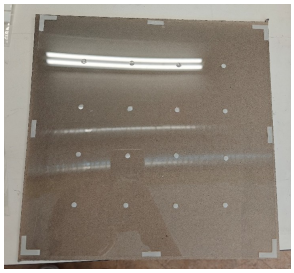

(a) Glass plate with 0.3 mm Mylar spacers (280×280 mm).

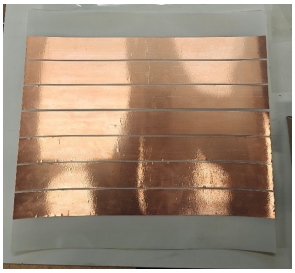

(b) Mylar sheet with seven copper strips, 2 mm spacing.

Figure 7: Layers used between the graphite electrodes

For the glass plate with spacers,we start from a 280×280 mm glass sheet. Mylar spacers of 0.3 mm thickness are cut and then glued to the designated face using a two-component glue (Fig. 7a). Positioning follows alignment marks to ensure planarity and uniform gap thickness. After gluing, the plate is left to dry, excess glue is removed and we check for any misalignment or missing areas. This operation is repeated for three glass plates, which are needed to build the complete detector stack. It is important that the plates are as identical as possible so that the gaps between layers are as uniform as possible.

The Mylar readout plane with copper strips is prepared on a 370×370 mm sheet. Seven 38 mm wide copper strips are cut to length, then placed and fixed on the Mylar with a constant 2 mm spacing between adjacent strips (Fig. 7b). The strips are kept parallel and centered on the sheet to obtain a regular pitch and good alignment. Bonding is done cleanly (no wrinkles or excess thickness) to preserve flatness. These copper strips provide the signal readout, and the seven strips correspond to the seven channels of the electronics OR of the digitizer.

II.3 Assembly of the MRPC Module

The assembly procedure aims to produce a geometrically stable and gas-tight stack while preserving the electrical properties of the resistive electrodes and the integrity of the readout.

II.3.1 Surface Preparation

All glass surfaces (resistive and transparent plates) were wiped with isopropyl alcohol and dried with lint-free wipes to remove dust, grease and moisture. Alignment marks on the frames and transparent plates were used to set the relative position of the components and to minimize cumulative misalignment across the stack.

II.3.2 Gluing and Stack Build-Up

A two-component epoxy adhesive was applied as a thin, uniform film *only* on the spacer contact areas and designated bonding lands, avoiding any spill into the gas gaps. The stack was built in the following order (Fig. 8) :

1. Bottom varnished glass panel ("black" glass, graphite-coated and insulated as described previously);
2. Three transparent glass plates carrying the Mylar spacers, stacked in the prescribed sequence to define the multigap geometry;
3. Top varnished glass panel("black" glass).

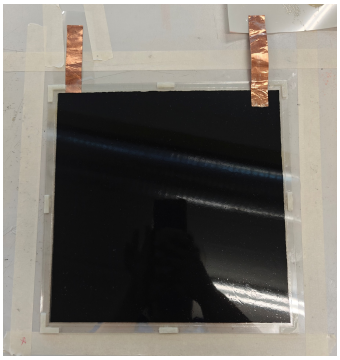

Figure 8: Final assembled MRPC module (top view).

After each bonding step, we use a flat weight to ensure planarity and to promote adhesive wetting. Excess squeeze-out at the edges was removed before cure. To avoid introducing residual stresses or tilt, only one layer was bonded per day and allowed to cure overnight.

II.3.3 Gas Interfaces and Readout Interconnects

The gas inlet and outlet fittings were glued into the dedicated openings and left until full cure. Electrical connections for the readout were then made by soldering the wires to the top and bottom copper strips (Fig. 9).

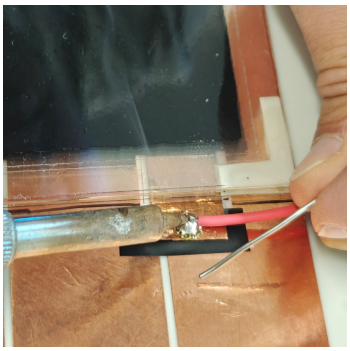

(a) Soldering the wire to a copper strip.

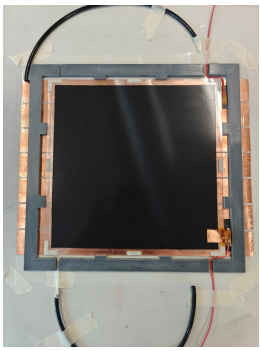

(b) Detector stack with frames and routing.

(c) Gas pipe glued into the port (close-up).

Figure 9: Assembly details: (a) wire soldering, (b) overall assembly, (c) gas connection.

All soldered joints were insulated with high-dielectric-strength tape (Kapton). Particular care was taken to avoid wrinkles or gaps that could trigger local discharges under high voltage and to prevent accidental shorts between adjacent strips.

II.3.4 Final Closure and Sealing

A Mylar sheet was bonded over the spacer perimeter to close the chamber. The entire outer perimeter was then sealed with silicone. This step is critical for long-term tightness: two passes were applied, excess material was removed and the seal was left to cure fully (Fig. 10).

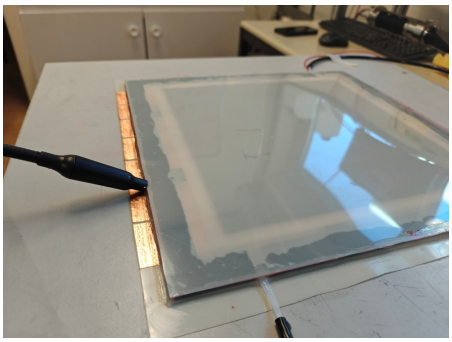

Figure 10: Detector sealed and leak test

Following cure, the detector was flushed with the selected gas mixture to purge air and dust from the gaps. Leak tightness was verified with a leak detector. Visual inspection confirmed planarity, correct alignment of the layers and cleanliness of the bonding lines. The module was then ready for high-voltage conditioning and subsequent performance measurements.

III Detector Analysis

III.1 Experimental setup

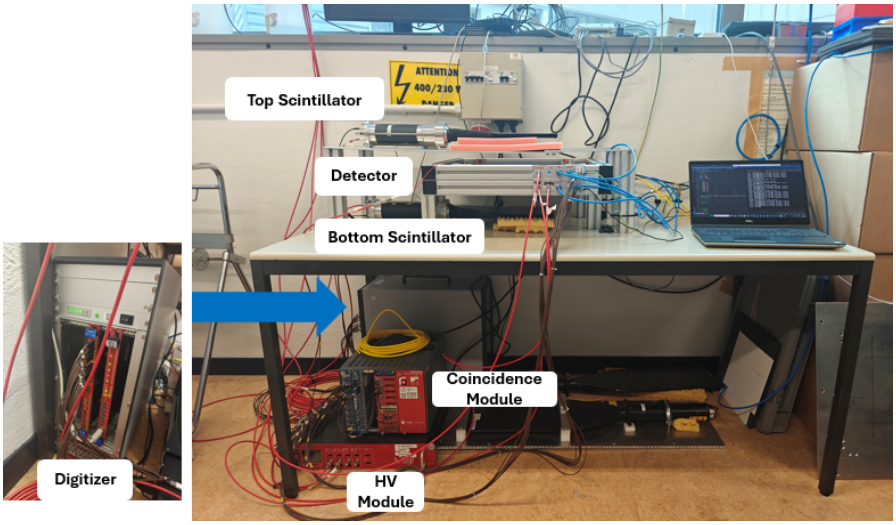

Figure 11: Cosmic-ray test setup

The setup consists of two scintillators one on top of the detector and the second one under (Fig. 11). The upper and lower scintillators provide the trigger. Their photomultiplier outputs are sent to a coincidence module, which delivers a logic trigger to the digitizer. A high-voltage (HV) supply biases the scintillators and the detector. The data-acquisition PC controls the digitizer and records the runs. Gas inlet and outlet lines are connected to the detector and routed to the facility gas system.

III.1.1 Scintillator calibration

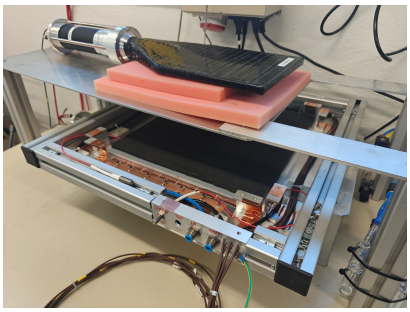

(a) Scintillator–MRPC stack during calibration.

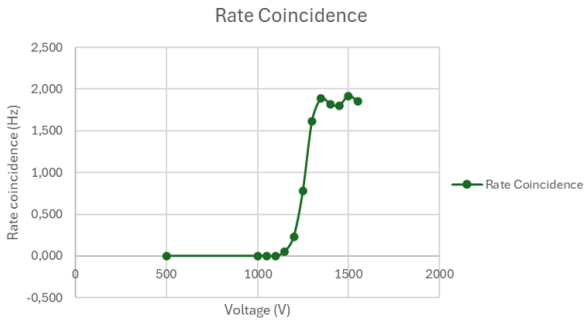

(b) Coincidence rate vs. HV

Figure 12: Scintillator calibration: setup and coincidence-rate curve.

Each scintillator is calibrated before installing the detector (Fig. 12a). First, the signals are checked on an oscilloscope to confirm coincidence presence. Then a coincidence–rate scan versus HV is performed: the HV is increased in steps while counting coincidences for a fixed time at each point (Fig. 12b). The working point is chosen on the plateau of the coincidence curve.

III.1.2 Detector installation in the setup

The MRPC module is mounted in its mechanical frame and centred between the scintillators. Gas tubes (inlet/outlet) are connected, the chamber is flushed to remove air and a quick leak check is performed. Readout connections are made by soldering the wires and resistors (50 Ω) to the copper strips (Fig. 13). The detector HV is then connected and kept on HV to get rid of impurities and dust. A short acquisition with the scintillator trigger confirms signal presence and time windows selection for the digitizer acquisition. After these checks, the setup is considered ready for systematic scans (HV, thresholds) and data taking.

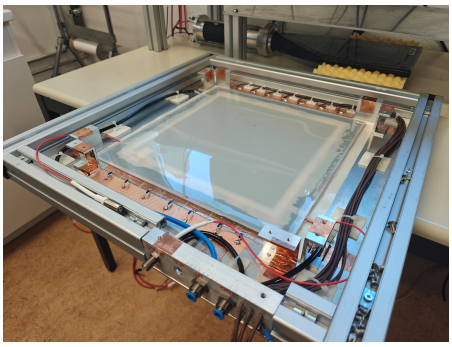

Figure 13: MRPC installed in the mechanical frame: gas ports, readout cabling and HV connections visible along the perimeter.

III.2 Weekly current scan and detector conditioning

HV	HV +	HV -	Current +	Current -	Current total
1000	500	500	0,02	0,02	0,04
2000	1000	1000	0,03	0,01	0,04
3000	1500	1500	0,03	0,01	0,04
4000	2000	2000	0,03	0,01	0,04
5000	2500	2500	0,03	0,01	0,04
6000	3000	3000	0,03	0,02	0,05
7000	3500	3500	0,03	0,02	0,05
8000	4000	4000	0,04	0,02	0,06
9000	4500	4500	0,04	0,03	0,07
10000	5000	5000	0,05	0,03	0,08
11000	5500	5500	0,05	0,03	0,08
12000	6000	6000	0,06	0,03	0,09
13000	6500	6500	0,07	0,04	0,11
14000	7000	7000	0,08	0,04	0,12
15000	7500	7500	0,09	0,07	0,16

(a) Table of current measurements.

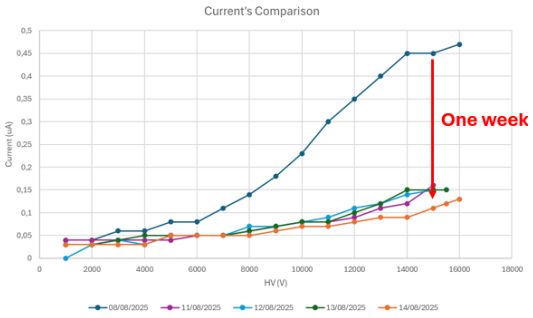

(b) Daily I–V curves over one week.

Figure 14: Weekly current scan used to condition and stabilise the detector.

To condition the chamber and stabilize its operating point, i performed a daily current scan over one week. Each day, the detector high voltage was increased stepwise from low bias to the nominal range (typically 1–15 kV) and the leakage/avalanche current was recorded at each step, producing an I–V curve (Fig. 14). Between scans, the detector was kept on at the "first-signal" high voltage during daytime to promote burn-in. The gas mixture was continuously flushed to remove residual air and outgassing products.

First, a progressive HV ramp helps to burn off residual dust or microscopic impurities and to complete the curing of interfaces and seals, which otherwise contribute to surface currents.

Second, repeating the scan over several days allows the current at a given high voltage to converge to a steady value, indicating that the detector surfaces and gaps have stabilized.

III.3 Efficiency analysis

III.3.1 Method

Two MRPC prototypes were tested independently. For each detector, an efficiency scan was performed with cosmic triggers from the scintillator. At each high–voltage (HV) step, about 1500 events were recorded and the efficiency was computed as

$$\varepsilon = \frac{N_{\text{hit}}}{N_{\text{trig}}},$$

where N_{hit} is the number of events with a valid MRPC signal and N_{trig} is the total number of coincidences. The scan started at the working point identified from the weekly current scan (around 14 kV), the voltage where stable signals first appear and proceeded up to ~ 18 kV.

III.3.2 Results

Figure 15 shows the efficiency as a function of HV for the two detectors. In both cases, the efficiency increases with HV but remains well below the performance of standard MRPCs (typically $\gtrsim 95\%$). A clear plateau is not reached; the maximum efficiency reached was around 40%.

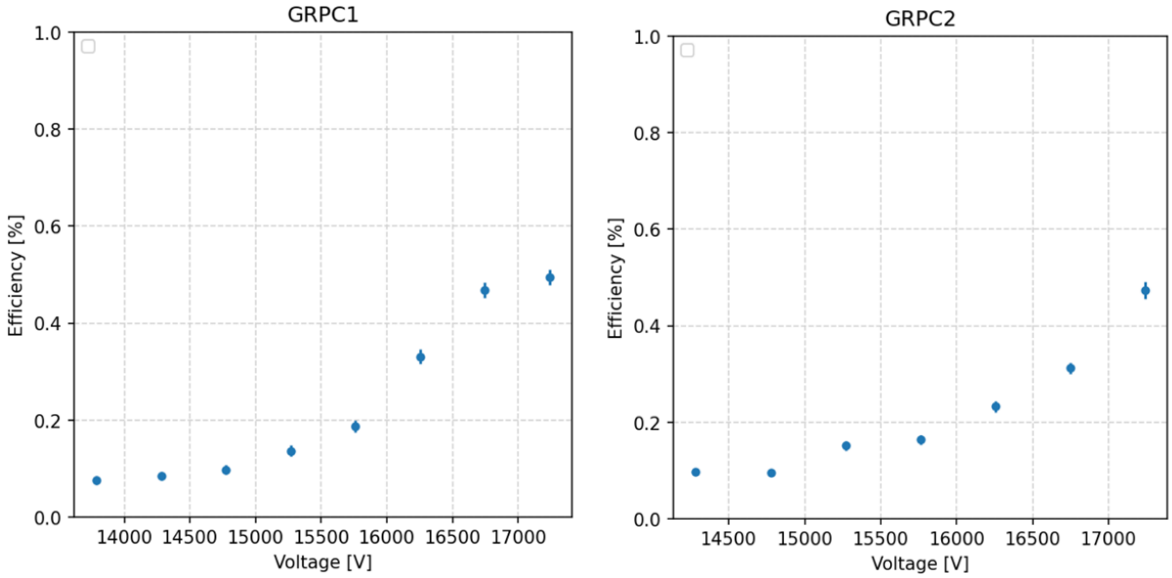

(a) MRPC1 : efficiency scan ($\sim$1.5k events per point).

(b) MRPC2 : efficiency scan ($\sim$1.5k events per point).

Figure 15: Efficiency versus HV for the two MRPC prototypes.

III.3.3 Operational limit and interpretation

The upper end of the scan is constrained by discharges close to $\sim$ 18 kV. At this point the chamber current exceeds the protection threshold and the HV trips, preventing further efficiency increase (Fig. 15). The same limitation is observed for both prototypes, which points to a constraint linked to the detector design or fabrication rather than an isolated defect. Because the plateau cannot be reached before the discharge threshold, the achievable efficiency remains low. Therefore, it is not possible to obtain reliable time-resolution data with these two prototypes, as the efficiency is too low. It is thus time to open both detectors to identify the root cause and determine whether it can be resolved.

III.4 Disassembly, Inspection, and Corrective Actions

III.4.1 Findings on MRPC1: bottom-glass fracture

Upon opening the first detector, a crack was immediately visible on the bottom glass plate (Fig. 16). After removing the stack from the peripheral supports, the fracture was located near the center of one side, very close to a spacer. Although multiple causes are possible, we know the glass was intact at installation. A plausible hypothesis is that the crack occurred during subsequent tests: when high voltage (HV) is applied, the structure experiences bending stresses which, above a certain HV, may exceed the strength margin for the given glass thickness. This detector is therefore not suitable for further improvement work.

Figure 16: Detector 1: fracture on the bottom glass near a spacer (highlighted in red).

III.4.2 Findings on MRPC2: non-uniform gaps and discharge hypothesis

The second detector showed no glass cracks and no burn marks on the graphite coating. However, inspection of the transparent-glass layers revealed that the inter-plate gaps were not uniform: the gap was larger in the central region than near the edges. This suggests that the number and/or distribution of spacers was insufficient to guarantee uniform planarity. Such non-uniformity can reduce efficiency (non-uniform gas flow and field), but it does not, by itself, explain the systematic discharge observed around 18 kV.

A second hypothesis was therefore formulated for the discharges: the clearance between the *top* graphite-coated glass and the closing Mylar sheet may have been too small. Since the Mylar is effectively at 0 V, an insufficient distance can favour local sparking to ground, leading to an HV trip near 18 kV.

III.4.3 Corrective actions and reassembly

To mitigate the suspected clearance issue, additional spacers of 4 mm thickness were glued on top of the existing ones, increasing the distance between the top graphite layer and the closing Mylar from about 1 mm to $\sim$ 5 mm (Fig. 17b). An extra coat of insulating (urethane) varnish was also applied to improve electrical insulation (Fig. 17a).

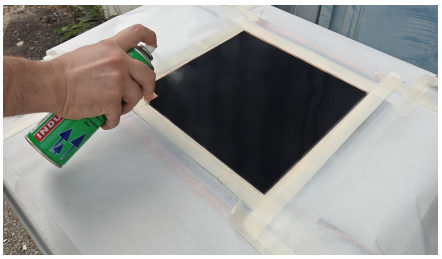

(a) Applying an insulating urethane (clear coat).

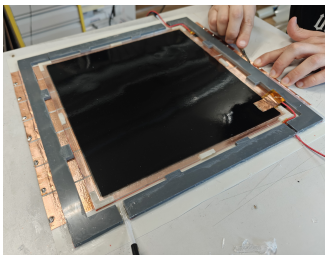

(b) Opening the detector for inspection and fixes.

Figure 17: MRPC rework steps: insulating varnish and detector inspection.

After these modifications, the detector underwent the full reassembly workflow: gluing and silicone sealing of the perimeter, installation into the mechanical frame, soldering of resistors and cables, connection of the front-end and HV and flushing with the selected gas mixture to purge air.

III.4.4 Post-repair tests

A new current scan and fresh efficiency measurements were then performed (Fig. 18). Unfortunately, the results did not improve significantly, which supports the conclusion that the uniformity of the glass-to-glass gaps is the dominant parameter affecting efficiency in these prototypes.

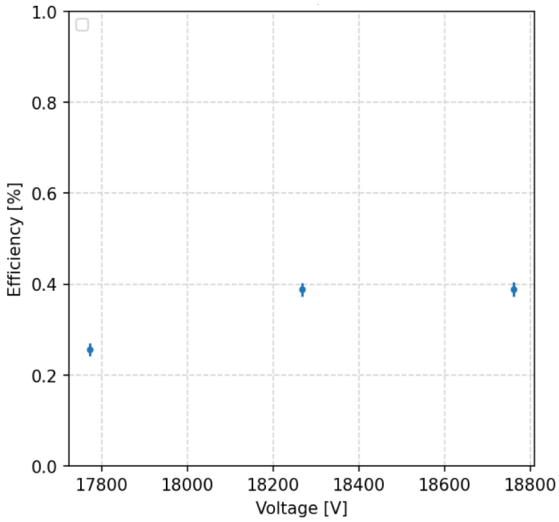

Figure 18: Post-rework efficiency scan (17.8–18.8 kV). The efficiency remains below $\sim$40%, confirming the limitation.

III.4.5 Next steps

These prototypes did not reach a performance level that allows a meaningful time-resolution study. However, the campaign validated the concept of routing gas around the detector (rather than only inside), which helped avoid excessive internal pressure and mechanical bulging. The work also clarified which design parameters most strongly affect behaviour (gap uniformity, spacer layout, dielectric clearances), providing concrete guidance for a redesign to prevent similar issues.

As a comparative reference, we plan to test an earlier detector built with another technique, in which gas flows only inside the chamber volume and not around it. This will help disentangle gas-routing effects from geometric and manufacturing factors.

III.5 Comparison of detectors

III.5.1 Design differences

We installed a MRPC built previously with another technique (Fig. 19). Compared with the two prototypes, this detector uses a larger number of spacers, which improves the uniformity of the gaps between glass plates. The gas routing also differs: the legacy chamber circulates gas only inside the active volume, rather than around the perimeter as in the prototypes. The overall mechanical stack is otherwise similar, but the denser spacer layout is expected to yield a flatter and more stable geometry.

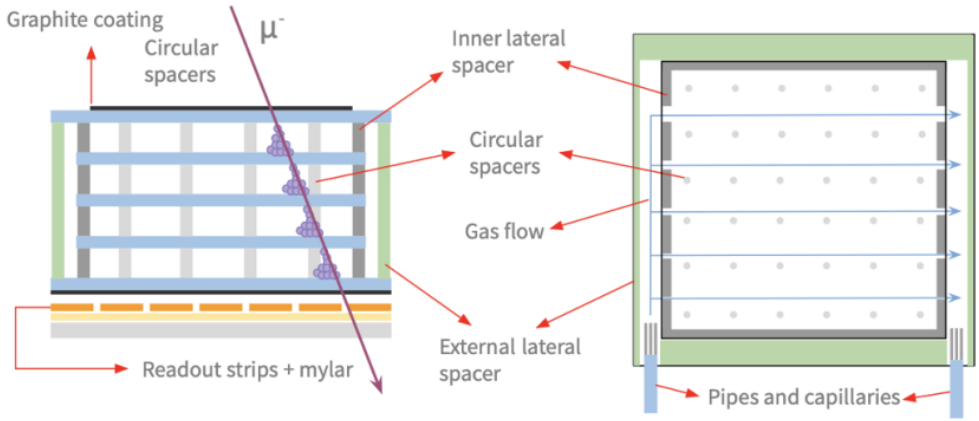

Figure 19: Previous MRPC schematic [6]

III.5.2 Installation and commissioning

The detector was mounted in the mechanical frame and went through the same preparation steps as before: soldering of resistors and wires, electrical connections and flushing with the selected gas mixture to purge air. After these procedures, the chamber was ready for tests (Fig. 20).

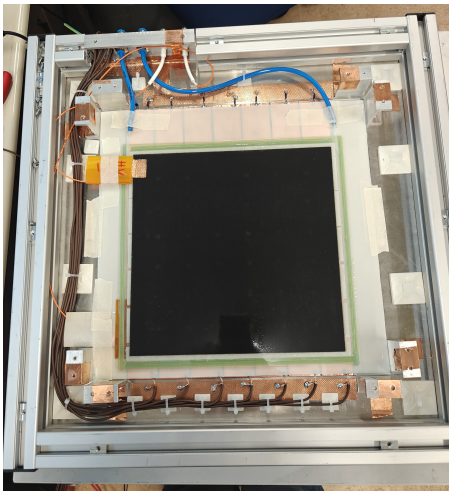

Figure 20: Previous MRPC installed in the mechanical frame: cabling, gas lines and readout visible along the perimeter.

III.5.3 Current scan

A current scan was performed by stepping the high voltage through the nominal range. The behaviour was stable across the scan, although the absolute currents were slightly higher than for the prototypes (Fig. 21).

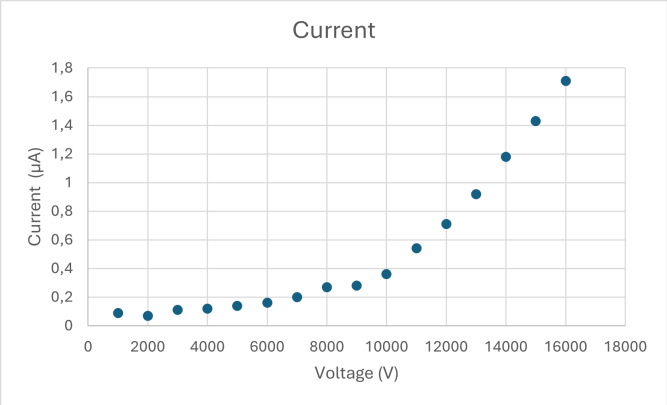

Figure 21: Current scan of the previous detector

III.5.4 Efficiency scan

An efficiency scan was then carried out using the scintillator. In contrast to the prototypes, the legacy detector reached a clear plateau at $\sim$ 70% efficiency. This constitutes a marked improvement and indicates that the detector can approach stable operation before the onset of discharges Fig. 22).

III.5.5 Interpretation and next steps

These results support the conclusion that gap uniformity driven by the number and placement of spacers is a key determinant of efficiency in this geometry. Going forward, we will use these

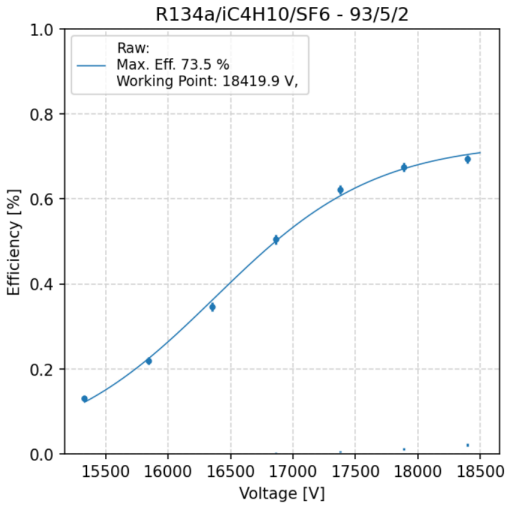

Figure 22: Efficiency scan of the previous detector (∼1500 events per point): plateau near 70% around 18 kV.

findings to design a new prototype that combines the advantages of both approaches: improved spacer density and placement to ensure uniform gaps, together with an optimized gas routing scheme. The objective is to raise the efficiency well beyond the present level and to enable robust time-resolution measurements.

IV Future Work and Proposed Solutions

IV.1 Prototype assessment and design implications

IV.1.1 Strengths and limitations of the prototype

The enclosure concept, in which the detector is housed inside a sealed box, proved effective at preventing overpressure in the chamber and limiting any mechanical bulging. From a practical standpoint, the prototype can be manufactured with commonly available materials and standard workshop tools. Most importantly, the device operates: clear signals are observed, which validates the basic working principle of the design.

Despite these merits, several weaknesses emerged. The assembly relies heavily on adhesive bonding, making the build essentially non-reversible and complicating inspection or rework. Moreover, the inter-glass gaps are not sufficiently uniform, a factor that directly limits the achievable efficiency. Finally, the fabrication workflow is slow: The curing and drying steps of glues, sealants, and coatings introduce long turnaround times between iterations.

IV.1.2 Design priorities for the next prototype

The next iteration should prioritize serviceability and geometric control. Adhesives should be minimized in favor of reversible joints, mechanical clamping with gaskets or O-rings, so that the chamber can be opened, inspected and repaired without damage. The number and distribution of spacers should be increased and optimized to obtain homogeneous gaps across the active area while preserving usable acceptance. In parallel, the mechanical design should be revisited to relate the bending loads applied during operation and testing to the selected glass thickness and frame stiffness to choose dimensions that raise the safety margin against deformation or cracking.

Addressing these points is expected to yield a higher efficiency by providing more uniform fields and gas flow. Even in the absence of immediate performance gains, a reversible construction will markedly shorten the development cycle, since opening and reworking the detector will no longer depend on lengthy curing periods between tests.

IV.2 Design improvements for future prototypes

IV.2.1 Motivation

The experience gained with the first two prototypes highlighted several limitations that must be addressed in future designs. The assembly process was extremely time-consuming, mainly due to the long curing times of the adhesives. Furthermore, the heavy reliance on glue made the construction non-reversible: Once glued, the chamber could not be opened or reworked and a broken glass plate meant that the entire detector became unusable. Another critical issue was the non-uniformity of the inter-glass gaps, which reduced performance and complicated alignment during stacking.

The next prototype must therefore focus on two priorities: reducing assembly time and making the detector fully reversible. Avoiding adhesives as much as possible is the key to this strategy.

IV.2.2 Proposed assembly concept

To achieve these objectives, a new mechanical concept has been developed. The idea is to use glass plates machined with small holes in predefined positions, through which alignment cylinders are inserted. These cylinders serve as guides for the precise stacking of all components. Thin spacers in the shape of washers are then slipped onto each cylinder in each layer, ensuring that the distance between successive glass plates is strictly defined by the washer thickness.

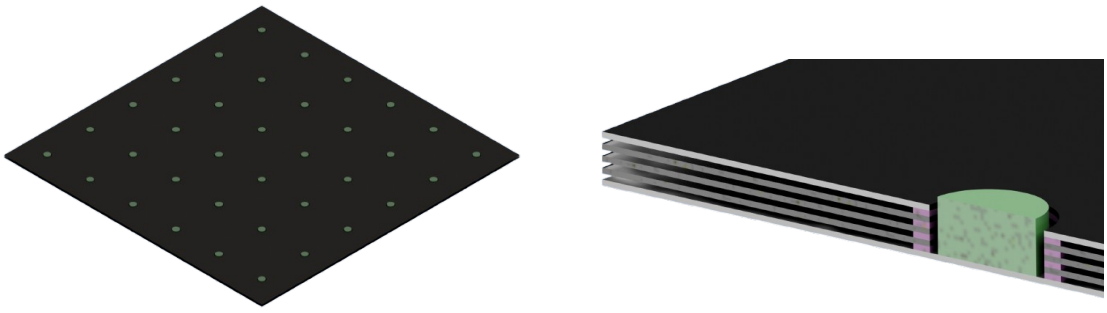

(a) Top plate view of the detector

(b) Half-cut view of the stacked glass layers with washer spacers (pink) guided by alignment cylinders (green).

Figure 23: New reversible assembly concept for the MRPC: uniform gaps enforced by washers and cylinders.

As illustrated in Fig. 23, assembly would begin with a graphite coated glass plate of dimensions 280×280 mm. On top of this, a drilled glass plate of the same dimensions is placed, followed by the insertion of the alignment cylinders. A washer is then added to each cylinder, after which the next glass plate is positioned. Repeating this process layer by layer creates a uniform stack until the final top glass plate, also coated with graphite and drilled to match the alignment scheme, is installed.

The fabrication of this concept appears feasible. Both the drilled glass plates and the washer-like spacers can be fabricated with high precision using laser cutting, which has already proven

reliable for thin components. The alignment cylinders can be ordered directly from specialized suppliers. The main challenge rely on the very small thickness of the elements: the glass and spacer washers are only 0.3 mm thick, meaning the complete detector stack remains mechanically delicate and relatively thin.

In this design, a total of 36 spacers are used, six per row, providing a sufficient distribution to achieve homogeneous spacing and good planarity throughout the active area.

IV.2.3 Concept of a 3D-printed support frame

A dedicated 3D-printed support could be designed to hold the four corners of the detector and prevent any relative motion of the stack during operation (see Fig. 24). Depending on the chosen material and plate thickness, it would be possible to incorporate tapped holes directly into the frame and to machine (or print) threads on the alignment cylinders, so that they can be simply screwed into the frame. This solution would secure the cylinders in place while keeping the assembly fully reversible.

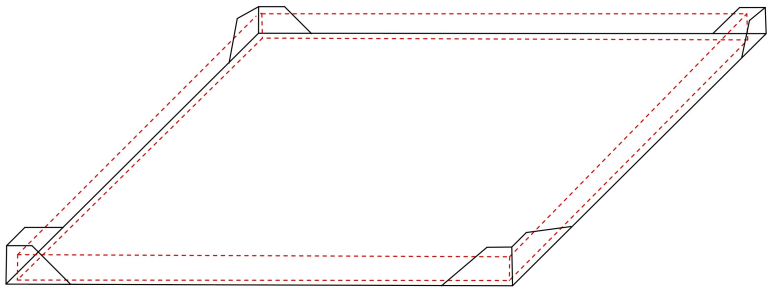

Figure 24: Concept of the 3D-printed support frame (black solid lines) with the detector outline indicated by red dashed lines.

The support could also be engineered to replace the external grey brackets currently used to keep the detector centred on the Mylar sheet with copper strips. In addition, the frame may include raised edges around the perimeter, effectively forming a shallow enclosure in which the detector is housed. Cable and gas-line routing can be integrated via dedicated through-holes and openings designed into the frame.

From a feasibility standpoint, the part can be split into four segments to fit the 3D-printer build plate and then assembled post-print. In summary, this approach would simplify assembly and minimize the use of adhesive in the fabrication process, thereby making each component serviceable and the overall detector easier to disassemble and rework.

V Conclusion

The work presented in this report has focused on the design, fabrication, and testing of glass multigap resistive plate chamber (MRPC) prototypes, with the dual objective of testing a new detector geometry and preparing a platform suitable for the evaluation of environmentally friendly gas mixtures. Two prototypes were designed and constructed, introducing the concept of circulating the working gas not only inside the detector but also around its volume, in order to mitigate overpressure effects.

The detectors were successfully assembled and commissioned.Their performance was studied through a series of systematic measurements, including current scans and efficiency scans. Although the prototypes were functional and signals were detected, their overall efficiency remained low, reaching only about 50% at best. Detailed inspections revealed structural issues, such as cracked glass and non-uniform inter-plate gaps, which limited the achievable performance and highlighted the limitations of adhesive-based assembly methods. These shortcomings prevented a meaningful study of time resolution, but they provided valuable feedback on the critical design parameters that govern detector behavior.

To address these challenges, several design improvements have been proposed. Chief among them are the elimination of irreversible adhesive joints, the introduction of mechanical alignment using drilled plates and washer-shaped spacers to guarantee uniform gaps and the reinforcement of the detector structure to better withstand mechanical stresses under high voltage. A comparison with a previous detector confirmed that greater spacer density and improved gap uniformity lead to higher efficiency, with values approaching 70%. This validates the central role of geometric precision and mechanical robustness in the performance of MRPCs.

While the prototypes developed during this project did not reach the efficiency levels required, they nonetheless provided critical insights into the relationship between detector design, assembly methods and performance. Indeed, they also validated the concept of a gas-distribution scheme surrounding the detector, which successfully prevented internal overpressure.

In conclusion, this project has established a solid foundation for the next generation of MRPC prototypes. The lessons learned on assembly techniques, material choices and gap uniformity will directly inform future designs, enabling more reliable, reversible and efficient detectors. These advances will, in turn, create a robust experimental platform for testing eco-friendly gas mixtures, ultimately contributing to CERN's broader efforts to reduce the environmental impact of gaseous detectors while maintaining high performance in demanding physics experiments.

References

[1] E. Cerron Zeballos, M. Abbrescia, G. Iacobucci, and et al. A new type of resistive plate chamber: The multigap RPC. *Nuclear Instruments and Methods in Physics Research Section A: Accelerators, Spectrometers, Detectors and Associated Equipment*, 374(1-2):132–136, 1996. doi: 10.1016/0168-9002(96)00158-1. URL https://www.sciencedirect.com/science/article/pii/0168900296001581.

[2] Regulation (eu) 2024/573 of the european parliament and of the council of 7 february 2024 on fluorinated greenhouse gases, amending directive (eu) 2019/1937 and repealing regulation (eu) no 517/2014. URL http://data.europa.eu/eli/reg/2024/573/oj. Legal status: In force.

[3] Kyoto protocol to the united nations framework convention on climate change. URL https://unfccc.int/resource/docs/cop3/l07a01.pdf. Adopted at the Kyoto Climate Change Conference, 10 December 1997.

[4] CERN. Cern environment report—rapport sur l'environnement 2021–2022. URL https://doi.org/10.25325/CERN-Environment-2023-003.

[5] B. Mandelli et al. Strategies for reducing the use of greenhouse gases from particle detectors operation at the CERN LHC experiments. 2374(1):012159. doi: 10.1088/1742-6596/2374/1/012159. URL https://doi.org/10.1088/1742-6596/2374/1/012159.

[6] Mattia Verzeroli. *Environmentally Friendly Gas Mixtures and Monitoring Systems for LHC Detectors*. Phd thesis, Université Claude Bernard Lyon 1 (Université de Lyon), Lyon, France, 2025. École doctorale n°52 — PHAST (Physique et Astrophysique de Lyon).